NWP SAF

Satellite Application Facility for Numerical Weather Prediction

Document NWPSAF-MO-VS-035

Version 1.2

11 December 2007

Incorporation of the JCSDA Zeeman RT model in RTTOV v9

Y. Han

NOAA/NESDIS Joint Center for Satellite Data Assimilation

EUMETSAT Met Office ECMWF KNMI METEO FRANCE Toujours un temps d'avance

NWP SAF Visiting Scientist Report

NWPSAF-MO-VS-035

Incorporation of the JCSDA Zeeman RT model in RTTOV v9

Y. Han
NOAA/NESDIS Joint Center for Satellite Data Assimilation
5200 Auth Road Camp Springs, 27640 U.S.A

This documentation was developed within the context of the EUMETSAT Satellite Application Facility on Numerical Weather Prediction (NWP SAF), under the Cooperation Agreement dated 1 December, 2006, between EUMETSAT and the Met Office, UK, by one or more partners within the NWP SAF. The partners in the NWP SAF are the Met Office, ECMWF, KNMI and Météo France.

Change record			
Version	Date	Author / changed by	Remarks
1.0	2.12.07	Y. Han	Initial draft
1.1	4.12.07	R. Saunders	Comments added
1.2	11.12.07	Y. Han	Revision (final)

Incorporation of the JCSDA Zeeman RT model in RTTOV-v9

TABLE OF CONTENTS

1. Introduction

The US Joint Center for Satellite Data Assimilation (JCSDA) has recently developed a fast radiative transfer (RT) model for SSMIS upper-atmosphere channels that are influenced by the Zeeman effect (Han et al., 2007). More recently, the work has been extended to assess and model the Zeeman effect for AMSU-A channel 14. This report provides a summary of the work performed at the UK MeOffice over a month period (October 18 – November 19, 2007) to implement the Zeeman models into RTTOV-v9.

The algorithms applied in the JCSDA Zeeman models for fast computations of atmospheric transmittances and radiances have many places in common with RTTOV. For instance, both models predict optical depths defined at fixed pressure levels, not at fixed levels of the integrated absorber amount as adopted by the Optical Path TRANsmittance (OPTRAN) model (McMillin et al., 1995). This feature allows the implementation to use a large portion of the computer code already in the RTTOV model. However, on the other hand, since these Zeeman affected channels are sensitive to the earth's magnetic field, new predictors and schemes have to be introduced. For example, the AMSU-A Zeeman model requires calculations of atmospheric transmittances at two orthogonal polarizations while the RTTOV's AMSU-A model computes only one component. To simplify the implementation, an averaged transmittance over the two polarization components may be used, but this approach may reduce the model accuracy. Thus, there is a trade-off between the model accuracy and code simplicity and efficiency.

The current Zeeman model for AMSU-A channel 14 should be considered as a prototype. It has so far not been thoroughly validated. Since the Zeeman effect is small, work also remains to check the impact of the Zeeman model in data assimilation applications by comparisons with the model without the inclusion of the Zeeman effect.

The report is organized as the following. The next section provides a description about the Zeeman effect on the channels considered here, followed by a section describing the model algorithms. Section 4 summarizes the implementation of the models into RTOV-v9. In the last section, important issues and remaining work are presented. The software items delivered to Metoffice are listed in Appendix A.

2. Effect of Zeeman-splitting on SSMIS and AMSU-A

In the 60 GHz frequency region, there is a cluster of O_2 magnetic dipole transition lines. These lines are usually designated as the $N+$ and $N-$ lines, representing respectively the transitions between the $J = N$ and $J=N+1$ and between $J=N$ and $J=N-1$ energy levels, where J is the quantum number of the total angular momentum and N (an odd number) is the quantum number of the rotational angular momentum. Figure 1 shows the 100 hPa level-to-space transmittance spectrum in this region. Further up in the upper stratosphere and mesosphere, the lines become sharp and a phenomenon called the Zeeman effect appears, induced by the interaction of the O_2 molecule's magnetic dipole moment with the earth's magnetic field. The energy level J splits into $2J+1$ new levels, associated with the azimuth quantum number M, which may take any integer number from $-J$ to J. The selection rules permit the $N+$ and $N-$ transitions for which the M number can either remain fixed or change by one. Thus, each of the $N+$ and $N-$ lines splits into three groups of sublines. The line components obtained when M is unchanged are called the π components. When M increases or decreases by one, the components are called the $\sigma+$ or $\sigma-$ components.

The three groups of components show different behaviours in polarization. The π components are linearly polarized in the direction perpendicular to the plane containing the magnetic field vector ***Be*** and the wave propagation direction ***k***. Their magnitudes reach a maximum when the angle θ_{Be} between ***Be*** and ***k*** is 90^o and become zero when the angle is zero. The σ+ and σ- components are respectively right and left circularly polarized when ***Be*** and ***k*** point in the same direction ($\theta_{Be} = 0^o$) and exchange the polarizations when ***Be*** and ***k*** point in the opposite direction ($\theta_{Be} = 180^o$). They become linearly polarized at $\theta_{Be}=90^o$ in the plane containing ***Be*** and ***k***. When the angle θ_{Be} takes other values, the polarization of the σ+ and σ- components are elliptical. Figure 2 shows an example of the Zeeman splitting effect: the original line is broadened by the spread of the sublines and the radiation becomes polarized.

The total splitting width (the spread range of the sublines) is about 0.5*Be* MHz, where *Be* is the strength of the earth's magnetic field, which may take a value in the range of 0.23 – 6.5 in Gauss unit near the earth surface. Thus, the Zeeman effect can only be observed by sensors with very narrow passbands on or near the centers of the unsplit *N*+ and *N*- lines and their sensitivity peak in the upper stratosphere and mesosphere. SSMIS channels 19 and 20 have passbands centered on the 7+, 9+, 15+ and 17+ transition lines with passband widths about 1 MHz, and therefore are strongly influenced by the Zeeman effect. The four passbands of channel 21 are located 2 MHz away from the centers of the 7+ and 9+ lines with passband widths similar to those of channels 19 and 20, and therefore is moderately influenced by the Zeeman effect. Channel 22 is 5.5 MHz away from the 7+ and 9+ line centers with passband widths twice of the size of the those in channels 19 and 20 and therefore the impact of the Zeeman effect is small. Channels 23 and 24 are further away from the line centers and the Zeeman efffect are insignificant. The effect of Zeeman splitting on channels 19-22 is illustrated in Figure 3, 4 and 5, which are computed using the US standard atmospheric profile shown in Figure 6 and the channel parameters listed in Table 1, which also includes those of AMSU-A channel 14. Note the vertical shifts (Figure 5) of the weighting function's peak heights when the earth magnetic field varies. The shifts and the temperature lapse rate shown in Figure 6 are largely responsible for the variations of the brightness temperatures (including both magnitude and direction of the changes) shown in Figure 3 and 4.

AMSU-A channel 14 has four passbands, 4.5 MHz away from the centers of the transition lines 11- and 13- with bandwidths of 2.9 MHz. Its sensitivity peaks around 40 km as shown in Figure 7. The impact of the Zeeman effect on this channel is revealed by the shift of the weighting function upward when the magnetic field strength *Be* increases. The impact is also illustrated in Figure 8, which shows its dependence on *Be*, θ_{Be} and the orientation of the receiver's polarization. As the figure shows, in theory it can have an impact up to 1K. However, in reality, the combination of the AMSU-A observation geometry and the orientation of ***Be,*** shown in Figure 9A and 9B, does not provide the conditions for the maximum impact to happen, as shown in Figure 9C. In these figures, the global distributions of the *Be* and $\cos(\theta_{Be})$ parameters on the AMSU-A pixels are computed from the data in the 1B data stream. Figure 9C shows the difference between simulated brightness temperatures with and without the inclusion of Zeeman effect. The variations of the receiver's polarization due to scanning have been taken into account. It can be seen that in the low latitude regions, although θ_{Be} can reach a value of 90^o, a condition for the maximum impact, the *Be* value is generally low, resulting in a relatively small impact. On the other hand, in the regions in which *Be* has large values (around 0.65 Gauss), the ***Be*** vector is near parallel with the **k** vector ($\theta_{Be} \approx 0^o$), resulting in a moderate impact compared with the maximum impact level which requires $\theta_{Be} = 90^o$.

SSMIS								
Ch	Passband 1		Passband 2		Passband 3		Passband 4	
	Offset (MHz)	BW (MHz)	Offset (MHz)	BW (MHz)	Offset (MHz)	BW (MHz)	Offset (MHz)	BW (MHz)
19	0 (15+)	1.34	0 (17+)	1.36				
20	0 (7+)	1.34	0 (9+)	1.37				
21	-2 (7+)	1.26	2 (7+)	1.23	-2 (9+)	1.33	2 (9+)	1.33
22	-5.5 (7+)	2.62	5.5 (7+)	2.61	-5.5 (9+)	2.66	5.5 (9+)	2.67
23	-16 (7+)	7.01	16 (7+)	7.17	-16 (9+)	7.40	16 (9+)	7.44
24	-50 (7+)	26.63	50 (7+)	26.33	-50 (9+)	26.04	50 (9+)	26.88
AMSU-A								
14	-4.5(11-)	2.9	4.5(11-)	2.9	-4.5(13-)	2.9	4.5(13-)	2.9

Table 1. Channel parameters. Offset – passband central frequency offset from the unsplit O_2 transition line center; BW – bandwidth. The line centers of the transitions, represented with 7+, 9+, 15+, 17+, 11- and 13- are 60.434776, 61.150560, 62.997977, 63.568518, 57.612484 and 56.968206 GHz, respectively. The SSMIS channels are left-circularly polarized, and AMSU-A channel 14 is linearly polarized – the polarization is normal to the scan plane when the antenna points at nadir (H polarization).

3. Fast radiative transfer models with the inclusion of Zeeman effect

3.1 Line-by-line base model

The fast RT models for SSMIS channels 19-22 and AMSU-A are based on the line-by-line (LBL) model Rosenkranz88 (Rosenkranz and Staelin, 1988). The LBL model uses a circular polarization basis and therefore it is a natural choice for SSMIS channels 19-22 which receive left circularly polarized radiation. The model solves the radiative transfer problem for the brightness temperature coherency matrix,

$$T_b = \begin{bmatrix} T_{b11} & T_{b12} \\ T^*_{b12} & T_{b22} \end{bmatrix}, \qquad (1)$$

where T_{b11} is the component of the right circular polarization, T_{b22} is the left circular polarization and T_{b12} is the coherency (the symbol * represents complex conjugate). The solution of the radiative transfer is given in a numerical form as

$$T_b = \sum_{k=1}^{N} (P_{k-1} P^+{}_{k-1} - P_k P^+{}_k) T_{a,k}, \quad (2)$$

where

$$P_0 = I, \quad P_k = P_{k-1} \exp(-G_k \Delta z_k), \quad (3)$$

G_k is the complex propagation matrix, $T_{a,k}$ is the temperature of the k^{th} layer, I is a unit matrix and Δz_k is the thickness of the k^{th} layer.

On a linear polarization basis, such as the one used for AMSU-A, the element T_{b11} in (1) is the brightness temperature with polarization along the **v'** axis in the coordinates system shown in Figure 10, in which the three vectors **v'**, ***h'***, and ***k*** form a right-handed orthogonal triad, with ***k*** points to the propagation direction and the (**v'**, ***k***) plane contains the earth's magnetic field vector ***Be***. It follows that the element T_{b22} is the component with polarization along the ***h'*** axis and the off-diagonal elements are the corresponding coherency. The RT solution of brightness temperature matrix with a linear polarization basis can be obtained from the solution on the circular polarization basis through a component transformation and is given by

$$T_{b\_linear} = C T_{b\_circular} C^{-1}, \qquad (4)$$

where

$$C = \frac{1}{\sqrt{2}}\begin{bmatrix} 1 & 1 \\ -i & i \end{bmatrix}. \quad (5)$$

AMSU-A channel 14 receives linearly polarized radiation whose polarization varies with scan angle θ_s from nadir. It is therefore necessary to transform the brightness temperature components defined in the coordinates shown in Figure 10 into a new coordinates system with the vertical and horizontal polarization defined in a usual way as shown in Figure 11. The result is (Stogryn, 1989),

$$\begin{aligned} T_{b,V} &= \cos^2\phi_{Be}T_{b,V'} + \sin^2\phi_{Be}T_{b,h'} - 2\sin\phi_{Be}\cos\phi_{Be}\,\mathrm{Re}\,T_{b,V'h'} \\ T_{b,h} &= \sin^2\phi_{Be}T_{b,V'} + \cos^2\phi_{Be}T_{b,h'} + 2\sin\phi_{Be}\cos\phi_{Be}\,\mathrm{Re}\,T_{b,V'h'} \quad , \quad (6) \\ T_{b,Vh} &= \sin\phi_{Be}\cos\phi_{Be}(T_{b,V'} - T_{b,h'}) + \cos^2\phi_{Be}T_{b,V'h'} - \sin^2\phi_{Be}T^*_{b,V'h'} \end{aligned}$$

where Re() is a function for taking the real part of the input variable and the other symbols are defined in Figure 11.

For AMSU-A channel 14, the third terms in the first two equations are not important (well below the 0.1 K level) and thus can be neglected. The brightness temperature that is measured by this channel is thus given by

$$T_b = \sin^2(\theta_s)T_{b,V} + \cos^2(\theta_s)T_{b,h}. \quad (7)$$

3.2 Fast models

For an atmosphere vertically divided into n+1 levels from the top of the atmosphere (TOA) to the Earth's surface, the solution for a brightness temperature component with a polarization p at frequency ν may be expressed as

$$T_{b,\nu,p} = \sum_{k=1}^{N}(\tau_{\nu,k-1,p} - \tau_{\nu,k,p})T_{a,k}\ , \quad (8)$$

where $\tau_{\nu,k,,p}$ is an apparent transmittance from level k to TOA, which was computed using Rosenkranz88, and $T_{a,k}$ is the mean temperature of the layer between levels k-1 and k. By averaging both sides of (8) over the channel's passbands we obtain the equation for the passband-averaged brightness temperature,

$$T_{b,ch,p} = \sum_{k=1}^{N}(\tau_{ch,k-1,p} - \tau_{ch,k,p})T_{a,k}\ , \quad (9)$$

where $\tau_{ch,k,p}$ is the passband-averaged (channel) transmittance. In the circular polarization basis, transmittance is a function of the geomagnetic field strength Be, the angle θ_{Be} between the magnetic field and wave propagation direction, and the air temperature. But on a linear polarization basis, the transmittance also in general depends on the azimuth angle φ_{Be} (see Figure 11). However, the φ_{Be} dependence can be ignored in the transmittance model by computing the transmittance in the special coordinates shown in Figure 10 (φ_{Be}=0). Then, the radiance at an arbitrary φ_{Be} value can be obtained by applying Equation 6.

A linear equation is developed to predict the k^{th} layer optical depth σ_k (for the convenience the symbol p for polarization is dropped),

$$\hat{\sigma}_k = c_{k,0} + \sum_{j=1}^{m} c_{k,j}x_{k,j}\ , \quad (10)$$

where $c_{k,j}$ are coefficients and $x_{k,j}$ are predictors. With the optical depth profile, the channel transmittances at a zenith angle θ_z are then calculated as

$$\hat{\tau}_{ch,k} = \exp(-\sum_{i=1}^{k} \hat{\sigma}_k / \cos(\theta_z)), \quad (11)$$

For the fast model developed at JCSDA, the atmosphere is divided into 100 fixed pressure layers with layer thicknesses of about 1 km and the top of the atmosphere set to 7×10^{-5} hPa (approximately at 110 km). The coefficients $c_{k,j}$ are obtained through regression. In the regression (training) process, the channel transmittances $\tau_{ch,k}$ are calculated from a set of diversified atmospheric profiles. The transmittances are then converted to the optical depth σ_k as

$$\sigma_k = \ln(\tau_{ch,k-1} / \tau_{ch,k}) \cos(\theta_z) \ , \quad (12)$$

which is the predictand in the training (dependent) data set. The UMBC 48 profile set (Strow et al., 2003) was adopted and extended to the required height from their original highest level of 0.005 hPa. For SSMIS channels 19 – 22, the training data set was prepared at three zenith angles confined to the range between 51° and 54° since the SSMIS scan angle is fixed at 45°, eleven points on *Be* ($20\leq B \leq 70$ μT) and 6 points on $\cos(\theta_{Be})$ ($0\leq\theta_{Be}\leq90^o$). For AMSU-A channel 14, the training data set was prepared in a similar way except that the zenith angle takes the values at air masses 1, 1.25, 1.5, 1.75, 2 and 2.5. The predictors were configured based in part on the radiance characteristics and in part on trial and error. Table 2 lists the predictors used for the fast RT models.

The fast model for SSMIS is tested against the base LBL model on an independent data ensemble. The ground-truth radiance data were simulated using the procedure discussed earlier. The temperature profile set consisted of 396 profiles from the empirical model, COSPAR International Reference Atmosphere (Fleming et al. 1988) (CIRA-88). The comparisons are shown in Figure 12. Also shown in the figure are the fitting errors (RMS differences on the dependent data set) and channel noise levels. The differences of the two models are well below the instrument noise levels. The model is also validated by comparisons between the simulations and measurements (Han et al., 2007). Figure 13a shows the scatter plots and statistics of the comparisons. The temperature profiles used for simulations are collocated retrievals from the limb-viewing infrared radiometric measurements by the Sounding of the Atmosphere using Broadband Emission Radiometry (SABER) on the Thermosphere-Ionosphere-Mesosphere Energetics and Dynamics satellite launched in December 2001 (Russell et al., 1999). Compared with the model without the inclusion of the Zeeman effect shown in Figure 13b, the differences are significantly reduced.

The fitting error for AMSU-A channel 14 is shown in Figure 14, plotted as a function of the top level set in the fast model (the top level for LBL model is fixed). The fitting error is about 0.035 K for the model with the top level set above 0.02 hPa level.

Channel	SSMIS
19, 20	ψ, ψBe^{-1}, $\cos^2(\theta_{Be})$, $\psi\cos^2(\theta_{Be})$, Be^{-1}, Be^{-2}, $\cos^2(\theta_{Be})Be^2$
21, 22	ψ, $\cos^2(\theta_{Be})$, Be, Be^3, $\cos^2(\theta_{Be})Be$, $\cos^2(\theta_{Be})Be^2$
	AMSU-A
14	ψ, ψ^2secant(θ_z),$\cos^2(\theta_{Be})$, Be secant(θ_z),Be^3, $\cos^2(\theta_{Be})Be^2$ secant(θ_z)

Table 2. Predictors. $\psi = 300./T_a$, T_a - air temperature; Be – geomagnetic field strength; θ_{Be} – angle between the geomagnetic field and wave propagation direction; θ_z - sensor's zenith angle.

4. Implementation of the fast models into RTTOV-v9

4.1 Model implementation for SSMIS channels 19 – 21

The Zeeman model requires the input atmospheric profile to reach a pressure level at least 0.0002 hPa (about 100 km), well above the top level required for the SSMIS channels currently being assimilated in the NWP models. To meet the requirement for the Zeeman channels and in the meantime not to alter the input profile structure for the other channels, channels 19-21 are treated separately through introducing a virtual instrument, named as ssmisz. The implementation is summarized below.

4.1.1 New instrument name and ID

Instrument name: *ssmisz*
Instrument ID: 36
Number of channels: 4 (SSMIS channels 19-22)

4.1.2 New coefficient file

Format: the RTTOV coefficient file format
Pressure levels: In the current implantation, the pressure levels listed in Table 3 are used.
Number of predictors:
Mixed gas: 11 (7 for channels 19 and 20 and 6 for 21 and 22, see Table 2)
Water vapour: 15 (the coefficients are all set to zero.)

Table 3. Pressure levels used for ssmisz

Pressure Level 0 (used in the training process) in hPa
0.0002
Level 1 – 62 (used in RTTOV) in hPa
0.0003 0.0010 0.0022 0.0050 0.0090 0.0161 0.0249 0.0384 0.0543 0.0769
0.1026 0.1370 0.1753 0.2244 0.2784 0.3454 0.4182 0.5064 0.6013 0.7140
0.8345 0.9753 1.1248 1.2972 1.4794 1.6872 1.9058 2.1526 2.4112 2.7009
3.3398 4.0770 4.9204 5.8776 6.9567 8.1655 9.5119 11.004 12.649 14.456
16.432 18.585 20.922 23.453 26.183 29.121 32.274 35.651 39.257 43.100
47.188 51.528 56.126 60.989 70.000 85.000 105.00 130.00 160.00 200.00
500.00 1013.00

4.1.3 Code changes

The flow chart in Figure 15 and Table 4 show the changes made in the rttov-v9 program to accommodate the Zeeman model.

Table 4. The source files and the changes made to these files.

Source file	Changes made
rttov_setpredictor.F90	Added a code segment to compute the predictors (see Figure 15)
rttov_setpredictor_tl.F90 rttov_setpredictor_ad.F90 rttov_setpredictor_k.F90	Made the corresponding changes following the changes for the FW routine
rttov_types.F90	Added scale variables Be and cosbk to the type definition of the profile_type structure to hold the values of Be and $\cos(\theta_{Be})$

rttov_const.F90	Added a scalar parameter to the instrument id list as inst_id_ssmisz=36 and a string item 'ssmisz' to the string array inst_name
rttov_direct.F90, rttov_tl.F90, rttov_ad.F90 and rttov_k.F90	Added the two code lines: linesProfiles_COEF(i) %Be = profiles(i)%Be Profiles_COEF(i)%cosbk=profiles(i)%cosbk

4.1.4 Test results

A test with a single profile is conducted to check the correctness of the implementation using the RTTOV tstrad program. The result is summarized in Table 5. Note that the differences in the brightness temperature of the forward calculations between the RTTOV and the JCSDA implementations are mainly the results of the differences in the pressures levels used in the fast transmittance models.

Table 5. Results of forward calculations using the RTTOV Zeeman model and those using the original Zeeman model as well as the outputs from the tstrad program running the RTTOV Zeeman model. The standard atmosphere (Figure 6) is used in the calculations.

FW calculation	Channel number 19 20 21 22 BT(RTTOV) 233.77 201.47 258.69 266.38 K BT(JCSDA) 233.81 201.42 258.72 266.40 K
TL vs Brute Force	PROFILE NUMBER= 1 TL= -0.4046157990E+01 BRUTE FORCE: -0.4046708433E+01 0.1000136041E+01 1 BRUTE FORCE: -0.4046211727E+01 0.1000013281E+01 2 BRUTE FORCE: -0.4046163351E+01 0.1000001325E+01 3 BRUTE FORCE: -0.4046158525E+01 0.1000000132E+01 4 BRUTE FORCE: -0.4046158022E+01 0.1000000008E+01 5 BRUTE FORCE: -0.4046157420E+01 0.9999998591E+00 6 BRUTE FORCE: -0.4046152640E+01 0.9999986776E+00 7 BRUTE FORCE: -0.4046137860E+01 0.9999950250E+00 8 BRUTE FORCE: -0.4045324431E+01 0.9997939875E+00 9 BRUTE FORCE: -0.4040430213E+01 0.9985843910E+00 10
TL vs AD	Differences are zero
TL vs K	Differences are zero

4.2 Model implementation for AMSU-A channel 14

4.2.1 Handling polarization

As described in Section 3.1, the original AMSU-A Zeeman model requires computations of transmittances for two orthogonal polarizations. This requirement is not consistent with RTTOV AMSU-A transmittance model, which computes only one transmittance component. To simplify the implementation, polarization is ignored in this implementation in the sense that only the following averaged transmittance is predicted

$$\tau = 0.5(\tau_V + \tau_h), \quad (13)$$

where τ_v and τ_h are transmittances of the two orthogonal polarizations. This is equivalent to setting the weights of the two brightness temperature components in Eq. (7) to a value of 0.5. With this approach the transmittance calculation and RT integration for this channel can be treated in the same way as the other channels. It appears that the approach of using the averaged transmittance profile does not significantly degrade the model accuracy (errors in

brightness temperature are about 0.1 K or less, depending on the geophysical location and sensor scan angle).

4.2.2 Predictors

The original Zeeman model and the RTTOV AMSU-A model both have temperature predictors, but with different forms. To minimize the number of new predictors, the two predictors ψ and ψ^2secant(θ_z) used in the original Zeeman model (Table 2) are replaced with the three predictors used in the RTTOV, secant(θ_z), *Ta/Tr* and $(Ta/Tr)^2$, where *Ta* is the air temperature and *Tr* is a reference temperature. The use of the new set of predictors does not significantly change the fitting error shown in Figure 14.

4.2.3 The *Be* and cos(θ_{Be}) parameters

The AMSU-A 1B data stream does not include the parameters *Be* and cos(θ_{Be}), but they can be derived from the data provided. The following is the steps to compute the two parameters.

(a) Compute the magnetic field vector ***Be*** using a lookup table (LUT), which contains pre-computed ***Be*** vectors (a snapshot of the field at a certain date and time) on the grid points of the latitude and longitude with a 2x2 degree grid size. The variation of the vector field with time is less than 2 % and is not important for this channel.

(b) Compute the sensor azimuth angle φ_{sat}, defined here is the angle on the local horizontal plane from the East to the projected line of the ***k*** vector, positive towards North. The 1B data stream provides a relative sensor azimuth angle φ_r, relative to the azimuth angle φ_{sun} of the Sun (see Figure 16), which is not included in the data stream. It is therefore necessary to compute φ_{sun} using the date and time information in the data stream. A program module *rttov_zutility* is included with RTTOV to compute φ_{sun}. The sensor's absolute azimuth angle is then computed as

$$\varphi_{sat} = 90 - (\varphi_r + \varphi_{sun}) . \quad (14)$$

(c) Compute ***k*** from θ_z (sensor's zenith angle) and φ_{sat}.

(d) Compute cos(θ_{Be}) and cos(φ_{Be}), as

$$\cos(\theta_{Be}) = Be \bullet k / | Be |$$

and

$$\cos(\varphi_{Be}) = Be_V / Be_p$$

where. Be_V is the component of ***Be*** on the axis of the vertical polarization V (see Figure 11) and Be_p is the component of ***Be*** projected on the plane containing the V and H vectors.

4.2.4 Code implementation

(a) The coefficient file

The number of predictors for mixed gas is extended to 14 from the original 10. For all channels except channel 14, the coefficients of the mixed gas predictors 11-14 are zero and for channel 14 the coefficients of predictors 5-10 are zero. Channel 14 shares the same predictors 1-4, as well as the pressure levels, with the rest of the channels.

(b) Code changes

The flow chart in Figure 17 and Table 6 show the changes made to accommodate the Zeeman model.

Table 6. The source files and the changes made to these files.

Source file	Changes made
rttov_setpredictor.F90	Added a code segment to compute the predictors (see Figure 16)
rttov_setpredictor_tl.F90 rttov_setpredictor_ad.F90 rttov_setpredictor_k.F90	Made the corresponding changes following the changes made for the FW routine
Rttov_types.F90	See Table 4
rttov_direct.F90, rttov_tl.F90, rttov_ad.F90 and rttov_k.F90	See Table 4
rttov_zutility.F90	A new module, which provides the following two functions: load_bfield() - a function to load the magnetic field lookup table compute_bfield - a subroutine with three forms to calculate $\boldsymbol{Be}$, $\cos(\theta_{Be})$ and $\cos(\varphi_{Be})$.

(c) Test results

(1) Code check

A test with a single profile is conducted to check the correctness of the implementation using the RTTOV tstrad program. The result is summarized in Table 7.

Table 7. The outputs from the tstrad program running the Zeeman model implemented in RTTOV.

TL vs Brute Force	PROFILE NUMBER= 1 TL= -0.3699026050E+02 BRUTE FORCE: -0.3672721800E+02 0.9928888716E+00 1 BRUTE FORCE: -0.3706866353E+02 0.1002119559E+01 2 BRUTE FORCE: -0.3699812066E+02 0.1000212493E+01 3 BRUTE FORCE: -0.3699104670E+02 0.1000021254E+01 4 BRUTE FORCE: -0.3699033920E+02 0.1000002128E+01 5 BRUTE FORCE: -0.3699026750E+02 0.1000000189E+01 6 BRUTE FORCE: -0.3699026752E+02 0.1000000190E+01 7 BRUTE FORCE: -0.3699018833E+02 0.9999980491E+00 8 BRUTE FORCE: -0.3698946216E+02 0.9999784176E+00 9 BRUTE FORCE: -0.3698659157E+02 0.9999008136E+00 10
TL vs AD	Differences are zero
TL vs K	Differences are zero

(2) Comparison with the original RTTOV (the Liebe's Zeeman correction term is removed)

The results are shown in Table 8. Note that the difference with (column 3 and 4) and without (column 2) the inclusion of the Zeeman effect increases as *Be* increases due to the shift of the weighting function peak height discussed in Section 2.

Table 8. Comparison of the forward calculations between the implemented RTTOV Zeeman model and the original RTTOV without the inclusion of Zeeman-effect (Liebe's Zeeman correction term in the line width is removed). The standard atmosphere shown in Figure 6 is used.

Zenith angle	No Zeeman	Zeeman, Be = 0.23	Zeeman, Be = 0.6
0^o	252.83 K	252.96	253.37
50^o	256.49	256.58	256.96

5. Summary and remaining issues and work

During the period from October 18 to November 19, work was completed at the Metoffice to implement into RTTOV-v9 the JCSDA fast radiative transfer models for SSMIS channels 19-22 and AMSU-A channel 14 that are affected by Zeeman splitting. The implementation for SSMIS treats the four channels as a separate sensor, named as ssmisz. A new coefficient file is created for this sensor. The implementation for AMSU-A, on the other hand, merges the coefficient data of the Zeeman model for channel 14 with those for the rest of the channels in the same coefficient file. Polarization is ignored, in the sense that only the average of the vertical and horizontal transmittance components is predicted. This approach simplifies the implementation with only a small reduction of the model accuracy (up to 0.1 K). The implementations of the two Zeeman models modify only a small portion of the computer code, mainly in the routines for the predictor calculations. A list of the routines and files modified is given in Appendix A. The implementations are tested with the RTTOV tstrad program with a standard atmospheric profile. The results show the computer codes for the tangent-linear, adjoint and k-matrix models are correctly implemented. The correct implementation of the forward model is checked by comparing the results with those from the original codes developed at JCSDA.

There are remaining issues and work, which are summarized below.

(a) The recent study has shown that the earth rotation can produce Doppler frequency shift as large as 65 KHz in low latitude regions and on the edges of the scan lines, causing an error of as large as 2K in these areas. To handle the shift at the RT model level is challenging because some of the parameters required for the calculations of the Doppler shift are not in the data stream. In addition, new variables must be introduced in the fast model. The symmetric properties of the passbands are destroyed, if the shift is not adjusted in the hardware level, which will invite the dependence of brightness temperature on the sign of $\cos(\theta_{Be})$. The current data records only stores the magnitude of the variable $\cos(\theta_{Be})$.

(b) In the model for SSMIS channels 19-22, a rectangular passband shape is currently assumed. However, there are other passband shape data sets. It is not clear which set is the one should be used. We recently tested a set of passband shapes, described as 'measured', in the file named SN2ffpb.dat. The use of this set of shape data reduces the difference between the model and measured radiances by about 0.4 K for channel 19 and makes little impact on the other three channels. More information is needed to address the passband shape issue.

(c) As indicated in the introduction, the current fast model for AMSU-A channel 14 should be considered as a prototype. Efforts will continue to validate it and refine the

algorithm. Ultimately, the need for the Zeeman algorithm will be evaluated through its performance in assimilating the data for NWP.

It is planned to incorporate the changes described here as part of the RTTOV-10 package currently under development to allow all users of RTTOV to be able make use of this option. Any users who want an early release of this code should contact the NWP SAF help desk at nwpsaf@metoffice.gov.uk.

6. Acknowledgements

I am sincerely grateful to Roger Saunders for providing the opportunity to visit the MetOffice and guidance for my work reported in this document. I would also like to thank Bill Bell for his help during my entire stay at Met Office, Peter Rayer for his technical support for this work, and John Eyre and Steve English for their comments on this work. The excellent collaboration with my colleagues at the MetOffice made my stay a valuable learning experience. Finally I would like to thank EUMETSAT for the financial support for the visit.

7. References

Fleming, E.L., S. Chandra, M. R. Shoeberl, and J. J. Barnett (1988), Monthly mean global climatology of temperature, wind, geopotential height and pressure for 0-120 km, *National Aeronautics and Space Administration*, Technical Memorandum 100697, Washington, D.C..

Han, Y., F. Weng, Q. Liu and P. van Delst (2007), A Fast Radiative Transfer Model for SSMIS Upper-atmosphere Sounding Channels, *J. Geophy. Res.*, **112**, D1121, doi:10.1029/2006JD008208.

McMillin, L. M., L. J. Crone, M. D. Goldberg, and T. J. Kleespies (1995), Atmospheric transmittance of an absorbing gas. 4. OPTRAN: a computationally fast and accurate transmittance model for absorbing gases with fixed and variable mixing ratios at variable viewing angles, *Appl. Opt.* **34**, 6269 - 6274.

Rosenkranz, P. W. and D. H. Staelin (1988), Polarized thermal microwave emission from oxygen in the mesosphere, *Radio Science*, 23, 721-729.

Russell, J. M., III, M. G. Mlynczak, L. L. Gordley, J. Tansock, and R. Esplin (1999), An overview of the SABER experiment and preliminary calibration results, presented at the 44th Annual Meeting, Int. Soc. For Opt. Eng., Denver, Colo., 18-23 July 1999.

Stogryn, A. (1989), The magnetic field dependence of brightness temperature at frequencies near the O_2 microwave absorption lines, *IEEE Transactions on Geoscience and Remote Sensing*, 27, 279-289.

Strow L.L., S. E. Hannon, S. D. Souza-Machado, H. E. Mottler, and D. Tobin (2003), An overview of the AIRS radiative transfer model," *IEEE Transactions on Geoscience and Remote Sensing*, 41, 303 – 313.

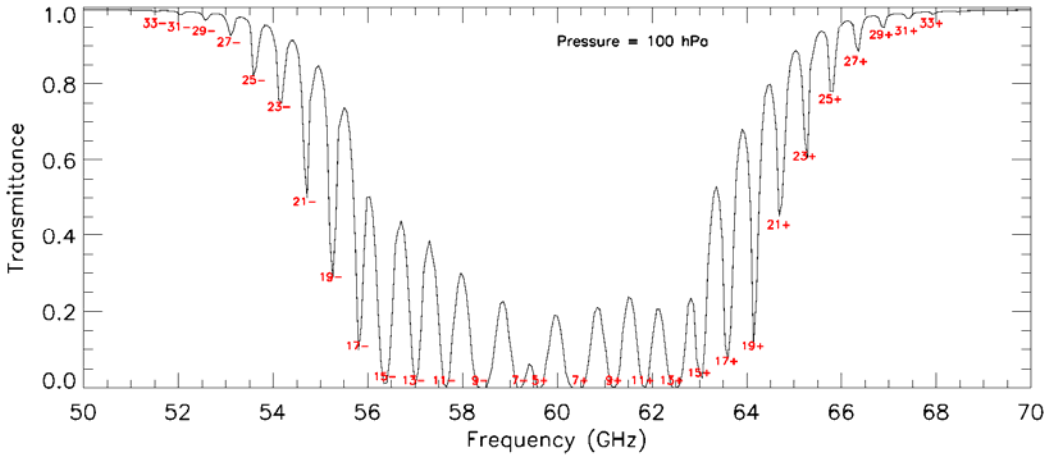

Figure 1. Oxygen level-to-space transmittance spectrum at pressure level 100 hPa.

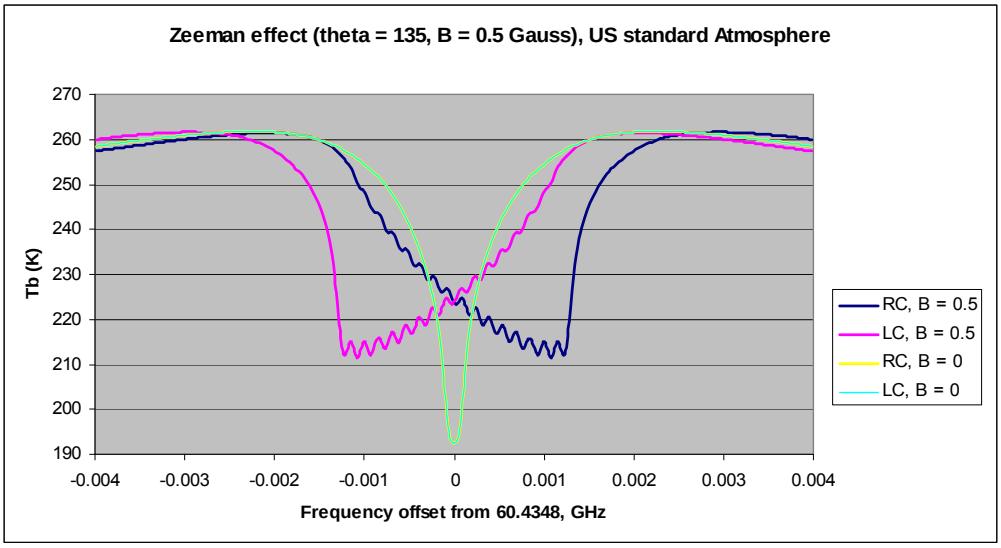

Figure 2. Upwelling brightness temperature spectrum near the 7+ line. RC – right circular polarization, LC – left circular polarization, B (*Be* in the text) – earth magnetic field strength and theta – the angle between the magnetic field and the wave propagation direction.

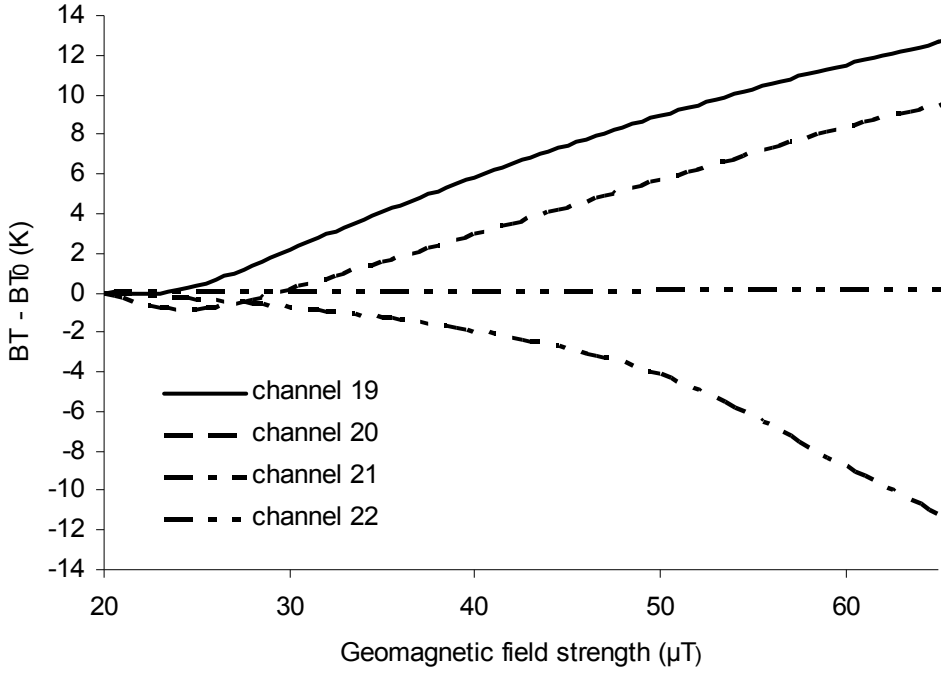

Figure 3. Brightness temperatures (BT) as a function of the geomagnetic field strength *Be* in unit μT (1 μT = 0.01 Gauss) with $\cos(\theta_{Be})$ fixed at 0.9. BT_0 = 230.3, 214.8, 259.9 and 258.6 K for channels 19 - 22, respectively.

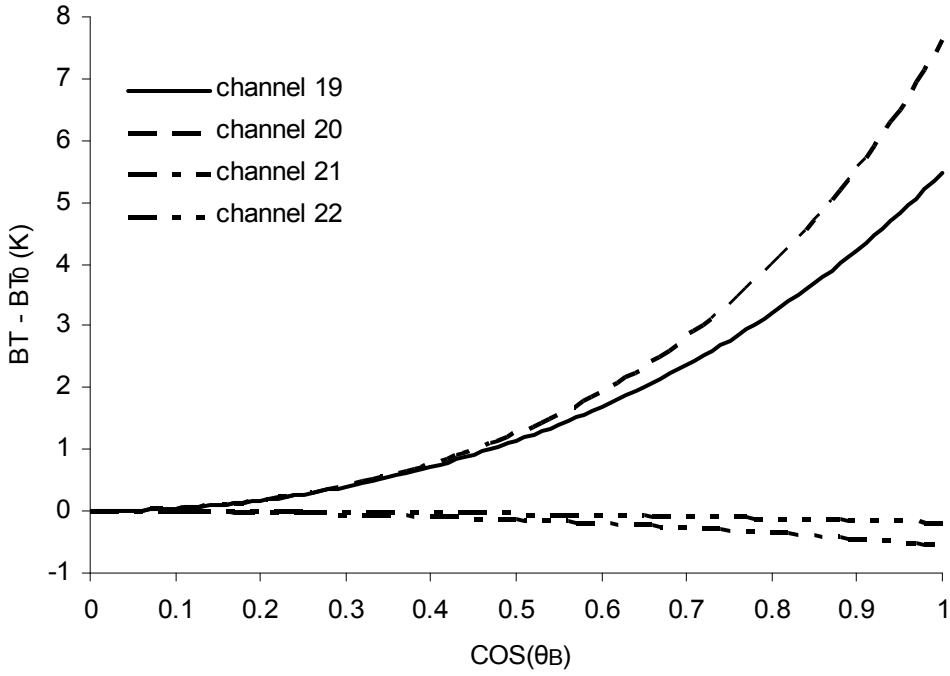

Figure 4. Brightness temperatures (BT) as a function of $\cos(\theta_{Be})$ with *Be* fixed at 60 μT (0.6 Gauss). BT_0 = 237.6, 217.6, 251.5, 258.9 K for channels 19 - 22, respectively.

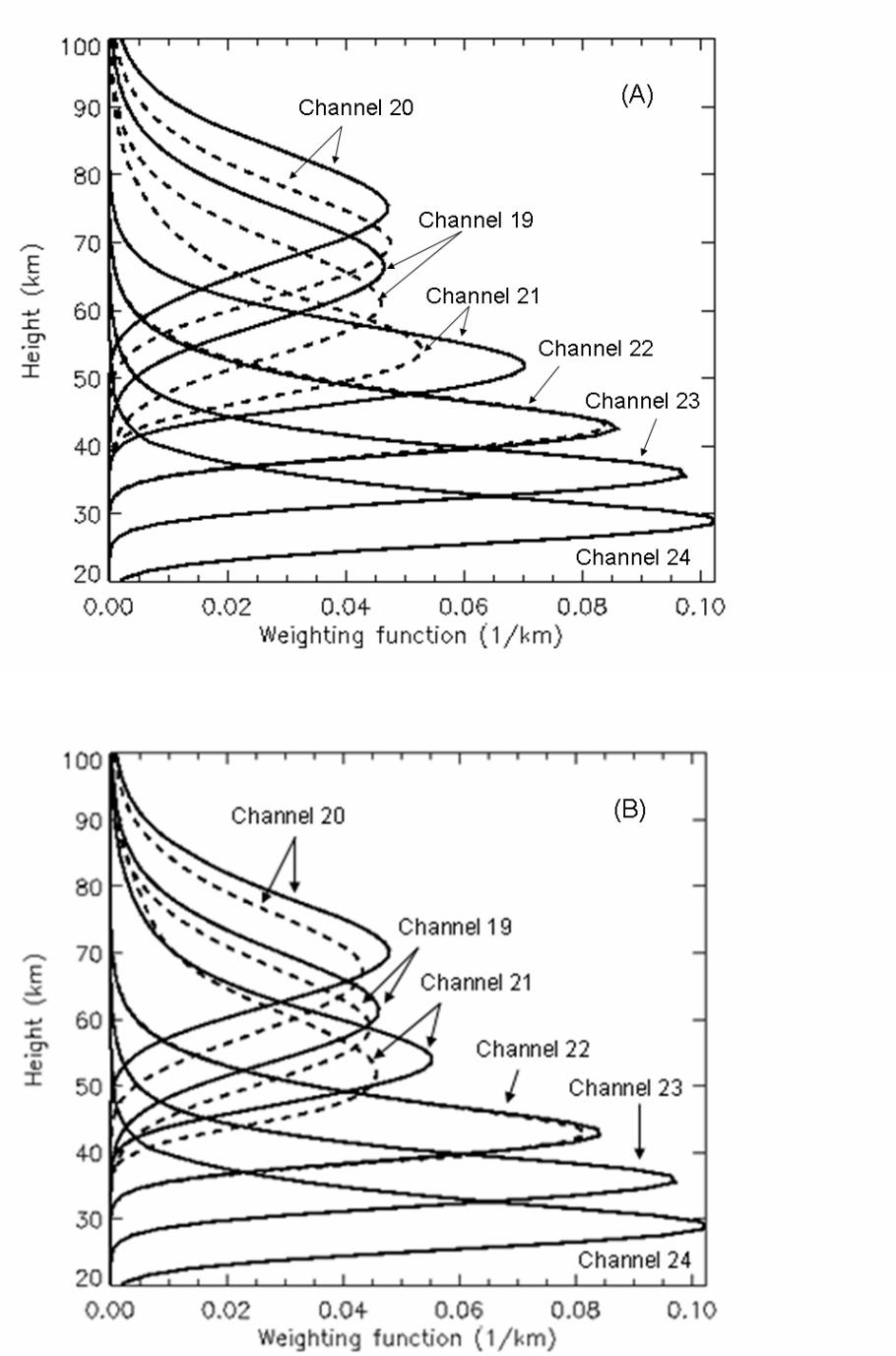

Figure 5. Weighting functions calculated with Be = 0.23 Gauss (solid lines) and 0.63 Gauss (dashed lines) at $\cos(\theta_{Be}) = 0.9$ (A) and with $\cos(\theta_{Be}) = 0$ (solid lines) and 1 (dashed lines) at Be = 60 μT (B), for the temperature profile of the US-76 standard atmosphere shown in Figure 6.

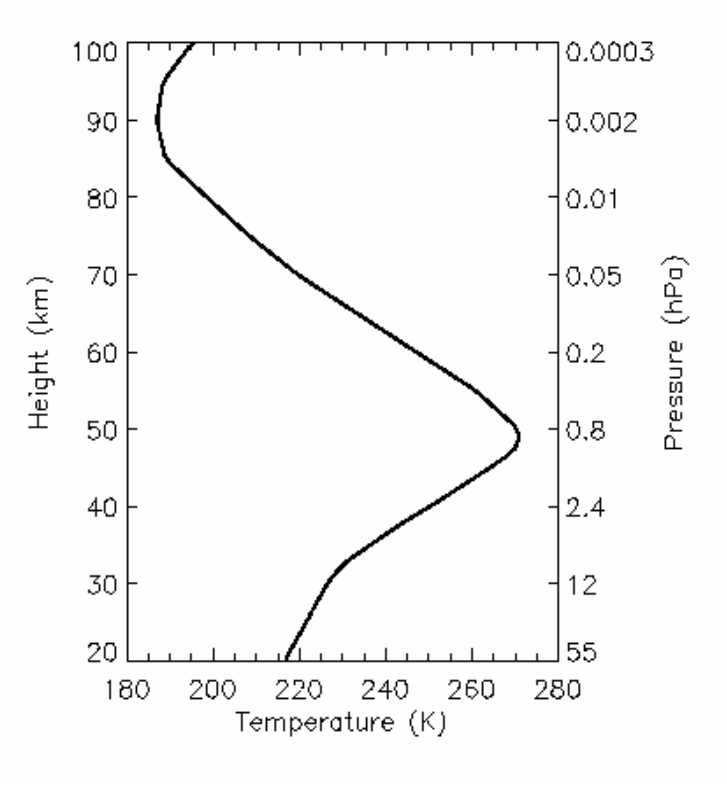

Figure 6. The 1976 US standard atmosphere.

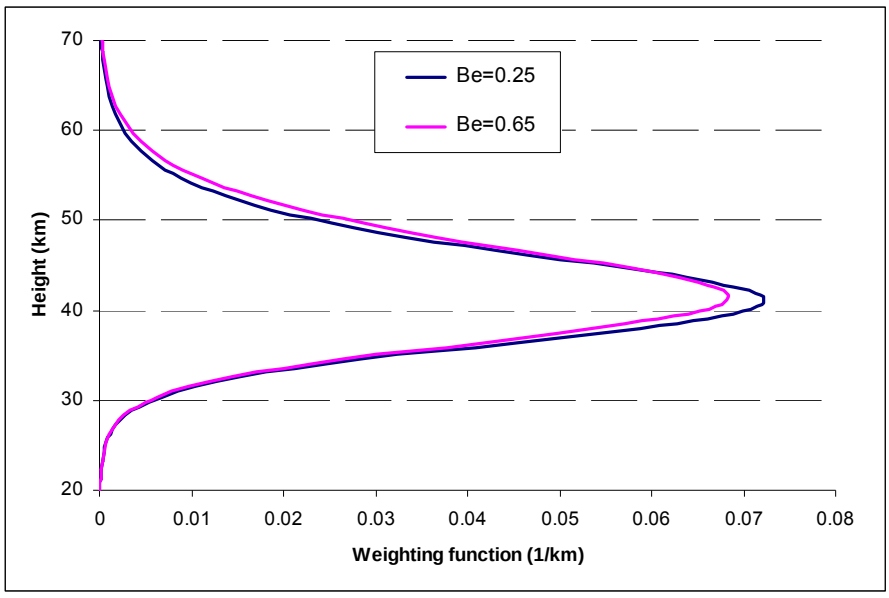

Figure 7. Weighting function of AMSU-A channel 14, calculated using the standard atmospheric temperature profile shown in Figure 6 at *Be*=0.23 and 0.65 in Gauss with $\cos(\theta_{Be})$=0 for the V' polarization component.

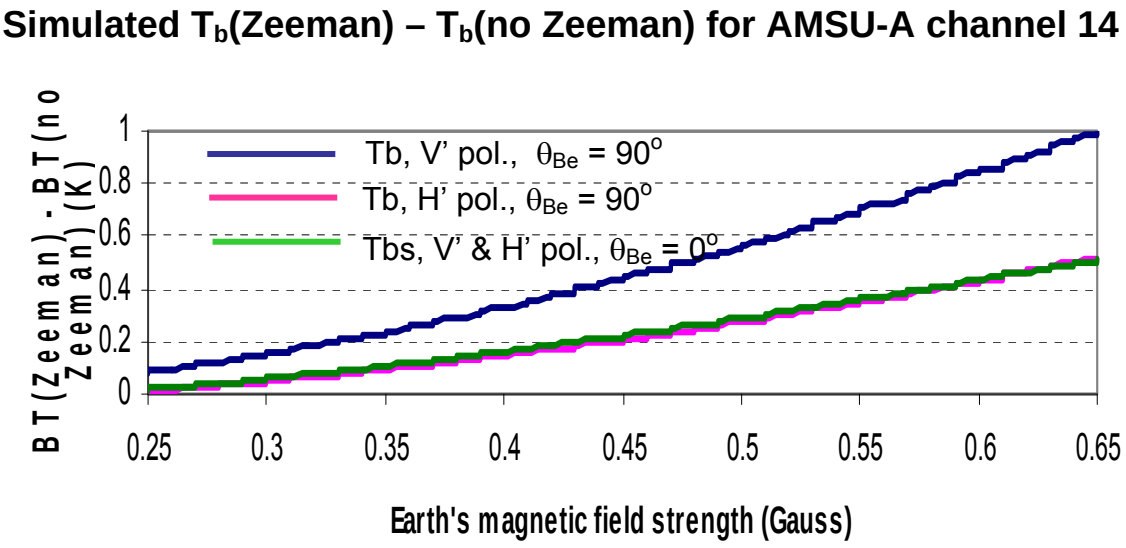

Figure 8. Differences of simulated brightness temperatures (BT) between the models with and without the Zeeman effect, using the temperature profile shown in Figure 6.

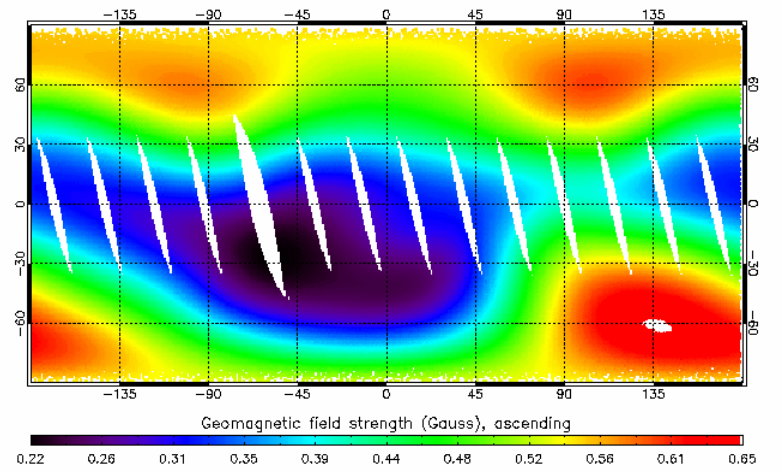

Figure 9A, Earth magnetic field strength *Be* at the pixels of AMSU-A ascending orbits, calculated using the 10th International Goemagnetic Reference Field (IGRF) model and the parameters in the 1B data stream.

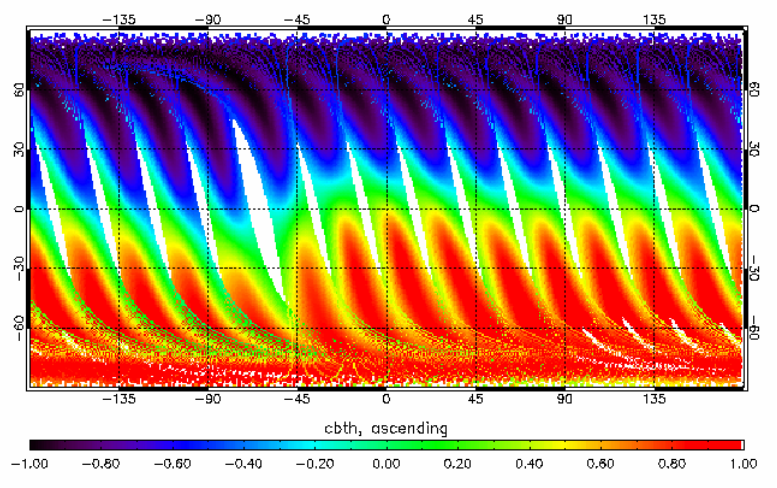

Figure 9B, The cos(θ_{Be}) field, i.e. the cosine of the angle between the Earth magnetic field and the wave propagation direction ***k*** at the pixels of AMSU-A ascending orbits, calculated using the 10th International Goemagnetic Reference Field (IGRF) model and the parameters in the 1B data stream.

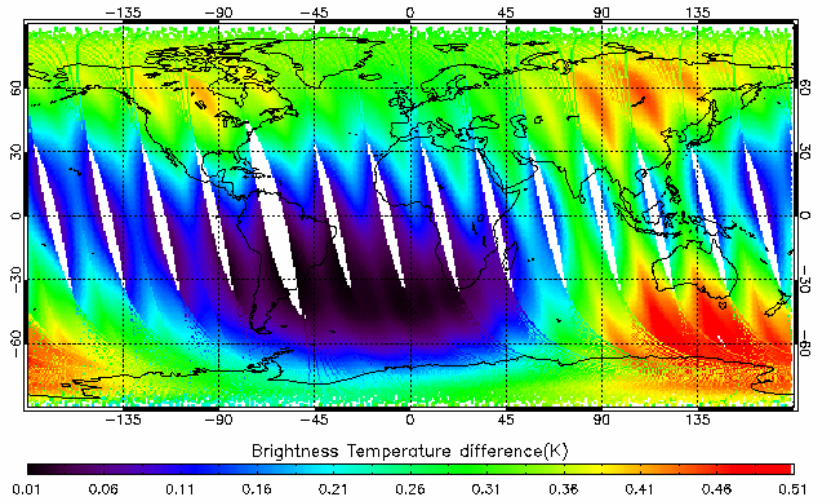

Figure 9C. Differences of the simulated brightness temperatures between the models with and without the inclusion of the Zeeman effect using the data shown in Figure 9A and 9B and the temperature profile shown in Figure 6 which is applied globally.

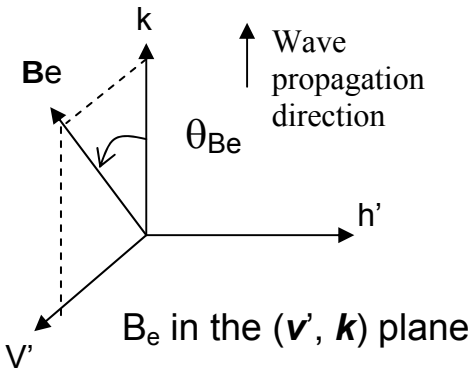

Figure 10. Coordinates with the three vectors **v'**, **h'**, and **k** forming a right-handed orthogonal triad.

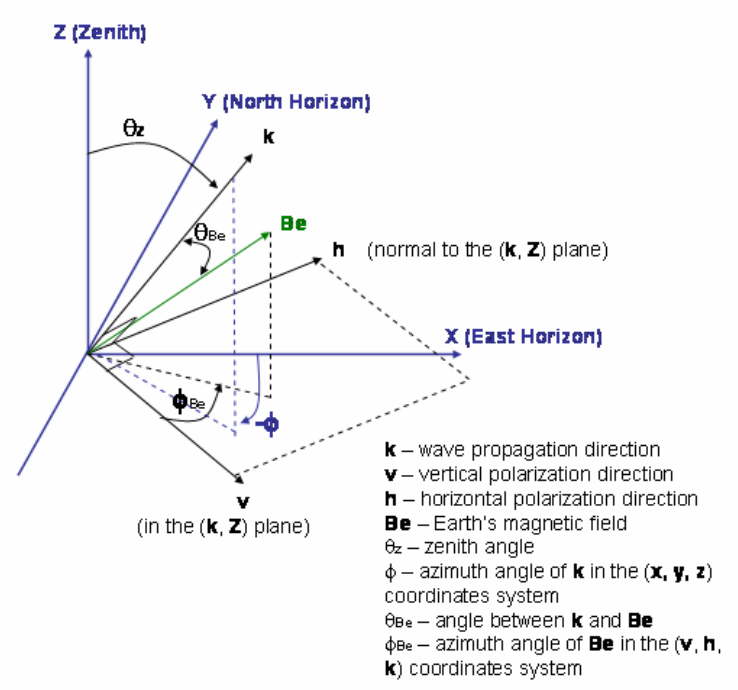

Figure 11. The AMSU-A oriented coordinate system.

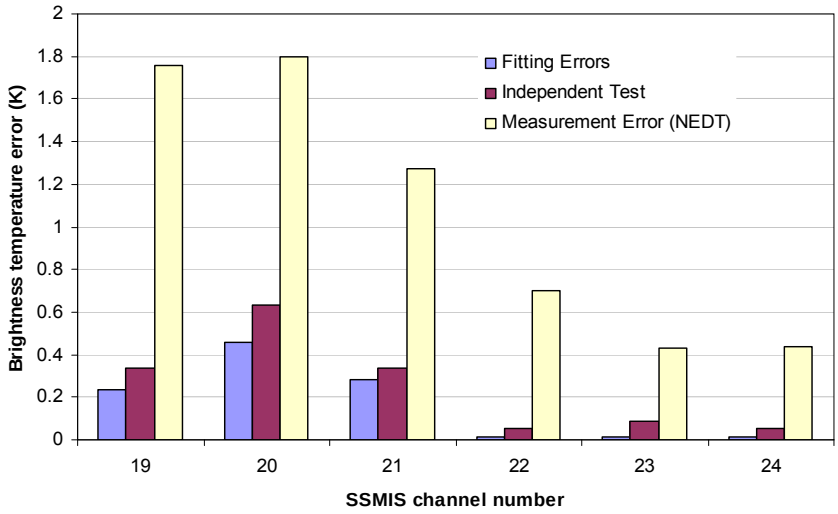

Figure 12. Root-mean-square differences between the fast model and base model on the dependent and independent profile sets and the instrument sensitivity (Noise Equivalent Delta Temperature).

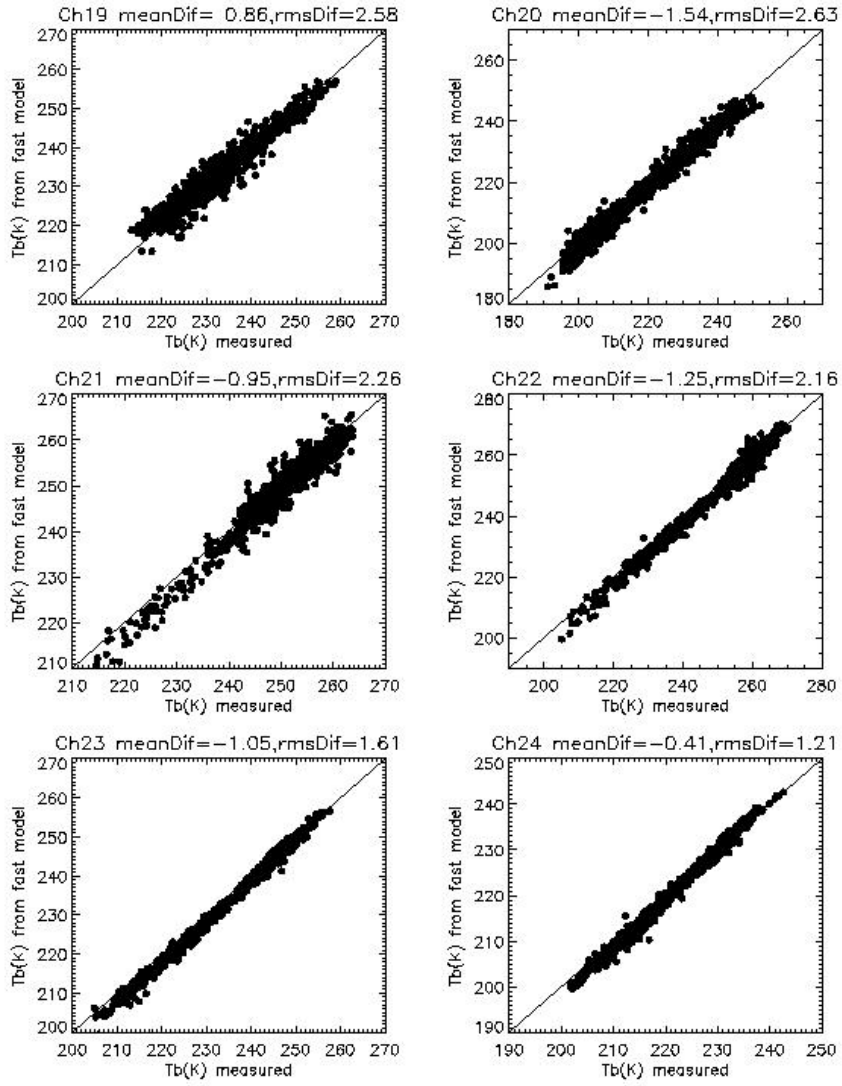

Figure 13A. Comparisons of brightness temperatures between the fast model and observations. The mean difference (meanDif) and root- mean-square difference (rmsDif) are displayed on the top of each figure. For the model calculations, the temperature profiles are those retrieved from the limb-viewing infrared radiometric measurements by the Sounding of the Atmosphere using Broadband Emission Radiometry (SABER). The SSMIS and SABER data are matched on the following criteria: an SSMIS pixel was collocated with a SABER profile if the absolute differences of the latitudes and longitudes between the two data points were less than 2 degrees, their distance was a minimum among all the data pairs, and the absolute time difference was less than 1.5 hour. Only nighttime data were used because of the possible contamination of solar radiation in the daytime SSMIS measurements. Data were taken from the SSMIS SDRs and SABER products on the following five days: October 25 and November 15 of 2005 and February 15, March 15 and April 15 of 2006. A total of 1097 matched samples are collected for the comparison. Of these samples, 304 are in high, 472 in middle and 321 in low latitude regions, and about half in the Southern hemisphere and half in the Northern hemisphere. In simulating the radiances, the atmosphere is assumed to be plane parallel and the zenith angles fixed at those near the WF peak heights.

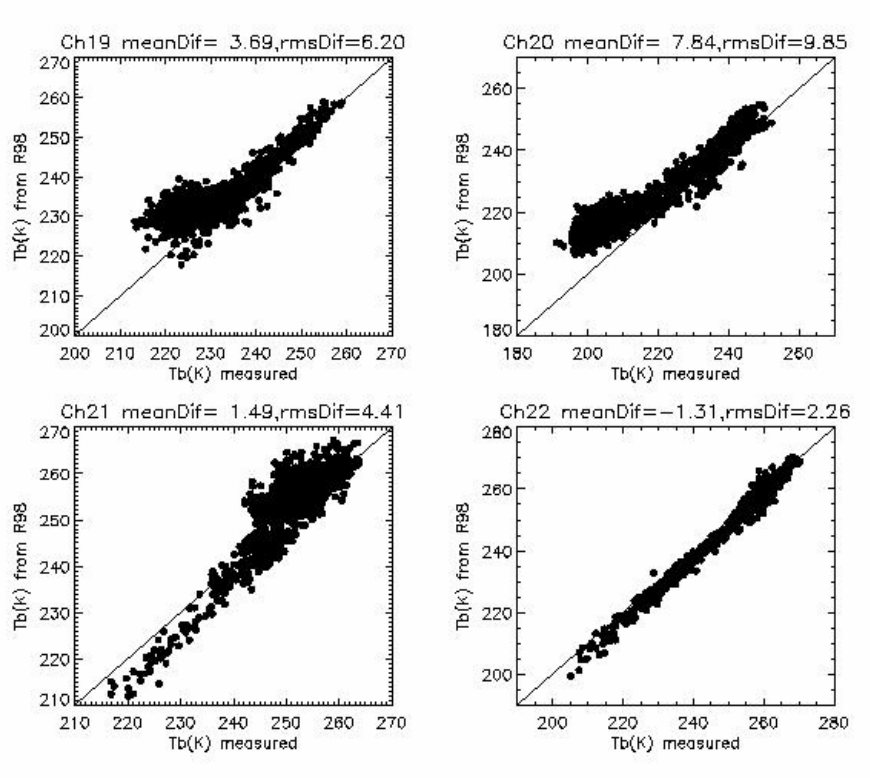

Figure 13B. Same as Figure 13A except that the comparisons are between the model without inclusion of the Zeeman effect and observations for channels 19 - 22.

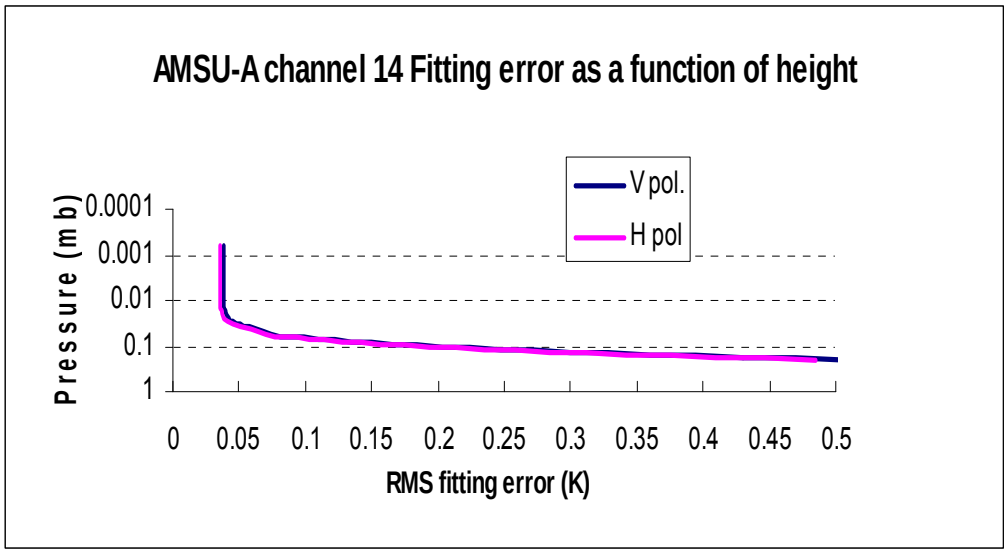

Figure 14. Fitting errors as a function of top pressure level set in the fast model for AMSU-A channel 14.

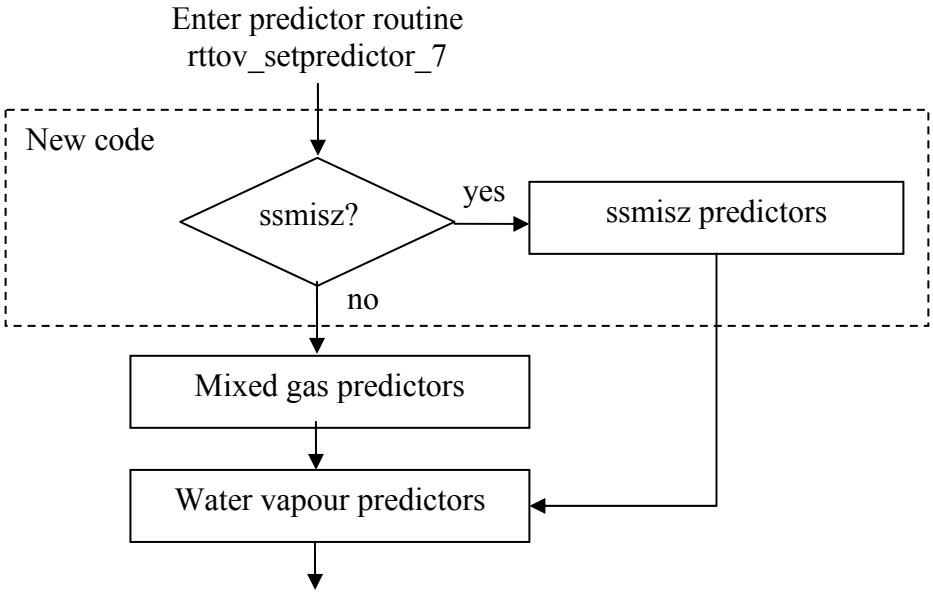

Figure 15. Flow chart of a program segment in the routine rttov_setpredictor_7. The code in the box with dashed lines is the code added to the routine for the SSMIS Zeeman model.

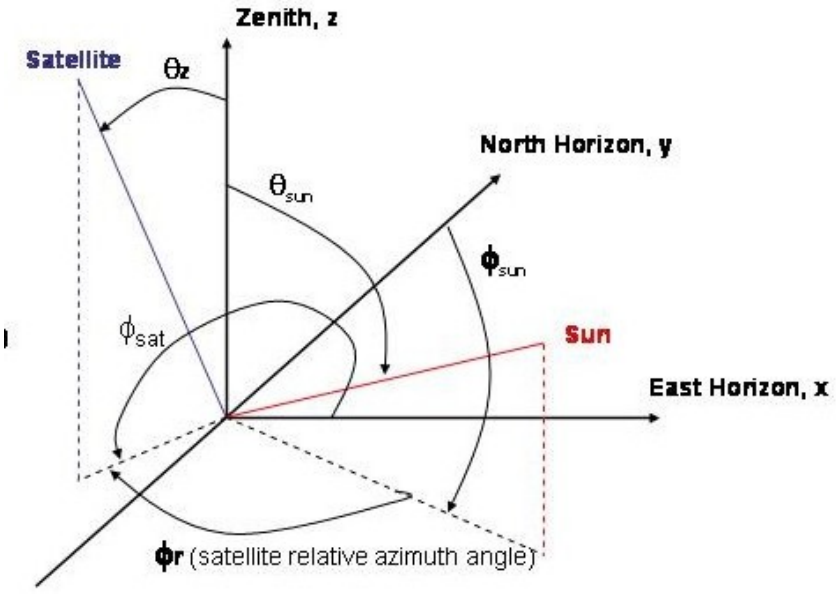

Figure 16. The relationship between the relative sensor azimuth angle and the azimuth angle of the Sun.

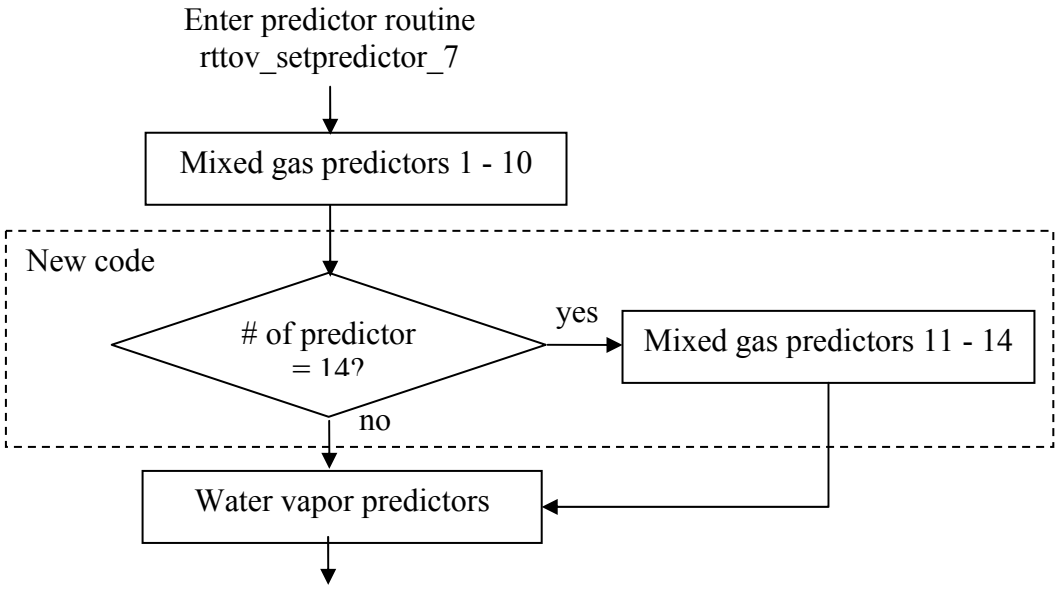

Figure 17. Flow chart of a program segment in the routine rttov_setpredictor_7. The code in the box with dashed lines is the code added to the routine for the AMSU-A Zeeman model.

Appendix A Items delivered to Met Office

(1) Modified RTTOV source files

(a) **rttov_setpredictor.F90:** added code segments to compute predictors for SSMIZ and AMSU-A channel 14.
(b) **rttov_setpredictor_tl.F90, rttov_setpredictor_ad.F90 and rttov_setpredictor_k.F90:** added codes corresponding to the changes made for rttov_setpredictor.F90.
(c) **rttov_types.F90:** Added scale variables *Be* and cosbk to the type definition of the profile_type structure to hold the values of Be and cos(θ_B) for both SSMISZ and AMSU-A channel 14.
(d) **rttov_const.F90:** Added a scalar parameter to the instrument id list as inst_id_ssmisz=36 and a string item 'ssmisz' to the string array inst_name.
(e) **rttov_direct.F90, rttov_tl.F90, rttov_ad.F90** and **rttov_k.F90:** added the two code lines to pass the Be and cosbk variables to the structure Profiles_COEF:
linesProfiles_COEF(i) %Be = profiles(i)%Be
Profiles_COEF(i)%cosbk=profiles(i)%cosbk

(2) New source files

rttov_zutility.F90: a Fortran module containing routines to compute *Be* and cos(θ_B) using the data from the 1B data stream.

(3) Coefficient files

(a) **rtcoef_dmsp_16_ssmiz.dat:** a new coefficient file for the SSMISZ sensor
(b) **rtcoef_metop_2_amsua.dat:** modified coefficient file for AMSU-A. The original coefficient data for channel 14 are replaced by those used in the Zeeman model.

(4) File containing the earth magnetic field lookup table

Be_LUT.2007.txt: a text file containing a lookup table of the earth magnetic fields computed for the date of January 1, 2007 at 00:00 UTC time using the IGRF-10 model.

(5) A software package containing modules and routines for line-by-line calculations of the channel transmittances and radiances for SSMIS channels 19-22 and AMSU-A channel 14 with/without the inclusion of Zeeman effect

(a) **radiance_ssmis.f90:** a module to compute channel (spectral response function averaged) transmittance and radiance for SSMIS channels 19-22.
(b) **radiance_amsua.f90:** a module to compute channel (spectral response function averaged) transmittance and radiance for AMSU-A channel 14.
(c) **ssmis_passband.f90:** a module containing data and routines to compute channel response functions from two sets of two passband shapes.
(d) **transmittance_microwave_lbl.f90:** a module to compute monochromatic transmittances with or without the inclusion of Zeeman effect for SSMIS channels 19-22 and AMSU-A channel 14.
(e) **A number of other source files containing modules and routines:** support the module defined in transmittance_microwave_lbl.f90.

(f) **SN2ffpb.dat:** a text file containing the SSMIS SN2 ffpb passband data (measured passband shapes).

Appendix B How to call RTTOV Zeeman models

(1) The interface to RTTOV Zeeman models remains the same as before except two new variables related to the earth magnetic field, added to the member list of the *profile* structure. The user needs to set the two variables profiles%Be and profiles%cosbk in the RTTOV interface argument list for SSMISZ and AMSU-A channel 14. Note that the *Be* variable holds the value of the earth magnetic field strength in Gauss unit and cosbk holds the value of **cos(θ_{Be})**, the cosine of the angle between the earth magnetic field vector ***Be*** and the propagation direction ***k***.

(2) For SSMISZ, the data for the *Be* and cosbk variables can be obtained from the SDR data stream. For AMSU-A, however, the data are usually not available from the data stream. To obtain them, the user may call the routines in the module rttov_zutility.F90. The usage is the following:

(a) Call the load_bfield_lut() routine to load magnetic field lookup table (need only once)
(b) Call the compute_bfield() routine to compute *Be* and cos(θ_{Be}), given the latitude, longitude, sensor zenith and relative azimuth angles, and date and time.

Detailed descriptions of their usage are in the source files. Examples of how to call these two routines are given below.

(a) Case when only a relative sensor azimuth angle is known

```
Program User_application_program

  USE rttov_zutility

  --- more codes here ---

  ! load geomagnetic field lookup table into module variables in module rttov_zutility
  ! fname_bfield_lut is the name of the data file containing the LUT

  error_status = load_bfield_lut('fname_bfield_lut')

  --- check the variable error_status ( 0 - success; 1 - error ) ---

  ! The following call may be repeated.

  latitude = 35.0_JPRB
  longitude = 135.0_JPRB
  sensor_zenang = 32.2_JPRB
  sensor_relative_aziang = 40.0_JPRB
  julian_day = 34_jpim    ! February 3 of the year
                          ! (1=Jan 1, 365=Dec31 (366 leap yr)*
  utc_time = 18.2_JPRB    ! 0 - 23.99999

   CALL compute_bfield(latitude,               &   ! input
                       longitude,              &   ! input
```

```
                      sensor_zenang,          &   ! input
                      sensor_relative_aziang, &   ! input
                      Julian_day,             &   ! input
                      utc_time,               &   ! input
                      Be,                     &   ! output
                      cos_bk,                 &   ! output
                      cos_bazi)                   ! output
 ! The output variables:
 !    Be - earth magnetic field strength (Gauss)
 !    cos_bk - cos(•Be)  see section 4.2 for definition
 !    cos_bazi - cos(φBe) see section 4.2 for definition

--- More code ----

END Program User_application_program
```

(b) Case when the sensor azimuth angle is known

Program User_application_program

USE rttov_zutility

--- more codes here ---

! load geomagnetic field lookup table into module variables in module rttov_zutility
! fname_bfield_lut is the name of the data file containing the LUT

error_status = `load_bfield_lut('fname_bfield_lut')`

```
--- check the variable error_status ( 0 - success; 1 - error ) ---

! The following call may be repeated.

latitude = 35.0_JPRB
longitude = 135.0_JPRB
sensor_zenang = 32.2_JPRB   ! sensor absolute azimuth angle
sensor_aziang = 100.0_JPRB

 CALL compute_bfield(latitude,               &   ! input
                      longitude,             &   ! input
                      sensor_zenang,         &   ! input
                      sensor_aziang,         &   ! input
                      Be,                    &   ! output
                      cos_bk,                &   ! output
                      cos_bazi)                  ! output
 ! The output variables: see example (a)

--- More code ----

END Program User_application_program
```

(c) Case to obtain earth magnetic field only

error_status = `load_bfield_lut('fname_bfield_lut')`

```
! The following call may be repeated

latitude = 35.0_JPRB
```

```
longitude = 135.0_JPRB

 CALL compute_bfield(latitude, longitude, & ! Inputs
                     Bx, By, Bz, Be)        ! Outputs
 ! The output variables:
 ! Bx  - East component of the magnetic field (Gauss)
 ! By  - North component of the magnetic field (Gauss)
 ! Bz  - Zenith component of the magnetic field (Gauss)
        Note Bz is positive when Be vector points upward
 ! Be  - the magnitude of the magnetic field Be
```